HHS Public Access

Author manuscript

Bioconjug Chem. Author manuscript; available in PMC 2024 April 15.

Published in final edited form as:

Bioconjug Chem. 2017 November 15; 28(11): 2865–2873. doi:10.1021/acs.bioconjchem.7b00566.

Evaluation of a Centyrin-based Near-infrared Probe for Fluorescence-Guided Surgery of Epidermal Growth Factor Receptor Positive Tumors

Sakkarapalayam M. Mahalingam[1,2], **Vadim Dudkin**[3], **Shalom Goldberg**[3], **Donna Klein**[3], **Fang Yi**[3], **Sunil Singhal**[4], **Karyn T. O'Neil**[3,*], **Philip S. Low**[1,2,*]

[1]Department of Chemistry, Purdue University, West Lafayette, Indiana 47907, United States

[2]Institute for Drug Discovery, Purdue University, West Lafayette, Indiana 47907, United States

[3]Janssen Research & Development, 1400 McKean Road, Springhouse PA 19477, United States

[4]Department of Surgery, University of Pennsylvania Perelman School of Medicine, Philadelphia, Pennsylvania 19104, United States

Abstract

Tumor-targeted near infrared fluorescent dyes have the potential to improve cancer surgery by enabling surgeons to locate and resect more malignant lesions where good visualization tools are required to assure complete removal of malignant tissue. Although the tumor-targeted fluorescent dyes used in humans to date have been either small organic molecules or high molecular weight antibodies, low molecular weight protein scaffolds have attracted significant attention because they penetrate solid tumors almost as efficiently as small molecules, but can be infinitely mutated to bind almost any antigen. Here we describe the use of a 10 kDa protein scaffold, a Centyrin, to target a near infrared fluorescent dye to tumors that over-express the epidermal growth factor receptor (EGFR) for fluorescence-guided surgery (FGS). We have developed and optimized the dose and time required for imaging small tumor burdens with minimal background fluorescence in real-time fluorescence-guided surgery of EGFR-expressing tumor xenografts in murine models. We demonstrate that the Centyrinnear infrared dye conjugate (CNDC) binds selectively to human $EGFR^+$ cancer cells with and EC_{50} of 2 nM, localizes to $EGFR^+$ tumor xenografts in athymic nude mice and that uptake of the dye in xenografts is significantly reduced when EGFR are blocked by pre-injection of excess unlabeled Centyrin. Taken together, these data suggest that CNDCs can be used for intraoperative identification and surgical removal of EGFR-expressing lesions and that Centyrins targeted to other tumor-specific antigens should prove similarly useful in fluorescence guided surgery of cancer. In addition, we demonstrate that the CNDC is detected in the NIR region of the spectrum and can be utilized for fluorescence-guided surgery (FGS). In addition, we propose that with its eventual complete clearance from EGFR-negative tissues and its quantitative

[*]**Corresponding Authors** koneil@its.jnj.com; plow@purdue.edu.

Supporting Information: This information is available free of charge via the Internet at http://pubs.acs.org

Conflict of Interest: This work was supported in part by a grant from On Target Laboratories. Dr. Philip Low is a co-founder and a member of the Board of Directors of On Target Laboratories.

retention in the tumor mass for >24 h, a Centyrin-targeted NIR dye should provide excellent tumor contrast when injected at least 6–8 h before initiation of cancer surgery in man.

Graphical Abstract

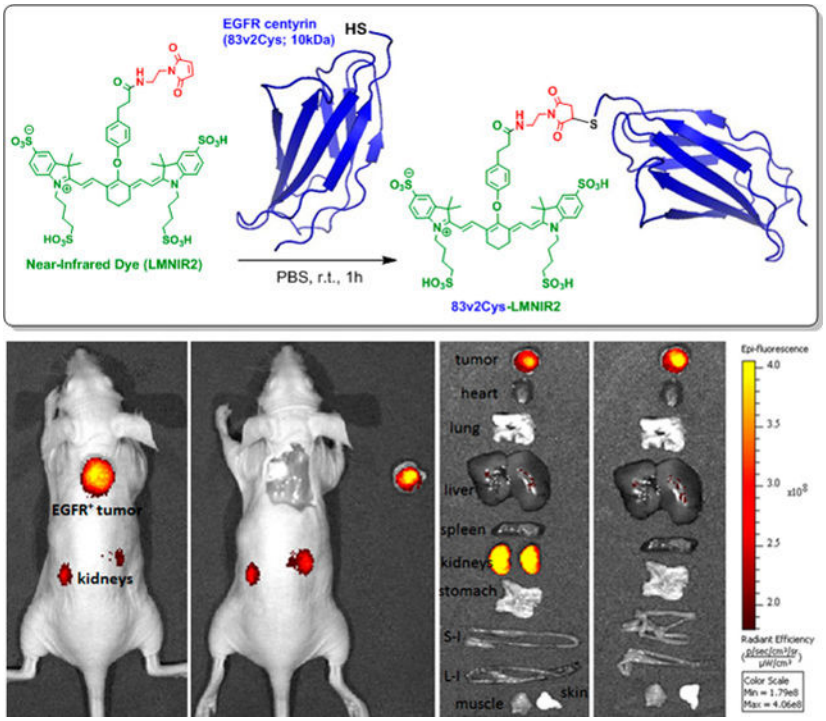

Introduction

Surgical resection constitutes the primary treatment for most solid tumors, since complete removal of all malignant disease remains the most effective cure for cancer. Although many imaging techniques are available for pre-operative diagnosis and staging of cancer, most of these imaging modalities cannot be used intra-operatively either because repeated exposure of the surgery staff to the associated ionizing radiation is too dangerous to the surgery staff, the time between data collection and image reconstruction is too long, or the mobility/flexibility of the imaging instrumentation is excessively cumbersome. As a consequence, surgeons must still rely primarily on subtle differences in tissue morphology, coloration, or rigidity to distinguish malignant from healthy tissues. While large tumor masses can be readily identified using these latter techniques, small malignant lesions, boundaries between cancer and healthy tissues, and buried malignant lymph nodes cannot be reliably distinguished by such methodologies.

Fluorescence-guided surgery is an emerging technique that uses either tumor-targeted or tumor-activated fluorescent dyes to illuminate cancerous tissues during surgery, allowing real time intra-operative localization of tumor nodules.[1] Our lab has previously developed fluorescent probes that are targeted to a folate receptor that is over-expressed in ovarian, lung, endometrial, kidney and other cancers.[2–4] Proof-of-principle studies in patients

with ovarian, lung, and kidney cancers have recently demonstrated that folate-conjugated fluorescent dyes can enable resection of significantly more malignant lesions than was possible by other standard techniques.[5–11] Unfortunately, folate receptors are only over-expressed in a subset of human cancers, raising the need for additional tumor-targeting ligands to deliver near infrared (NIR) fluorescent dyes to folate receptor negative cancers.

The human epidermal growth factor receptor (EGFR) is known to be over-expressed in many types of cancers, including cancers of the head and neck, pancreas, lung, colon, breast, and ovaries among others.[12, 13] Although currently available monoclonal antibodies to EGFR show high affinity and specificity for the aforementioned malignancies, they do not constitute ideal ligands for fluorescence-guided surgery because they clear too slowly from EGFR-negative tissues for use during same-day surgeries[14–16] and often do not yield the tumor contrast of smaller molecular weight targeting ligands[5–11]. While a low molecular weight EGFR-specific organic molecule could conceivably be exploited to deliver a fluorescent dye to EGFR-expressing tumors, no EGFR-specific ligand exists that both binds an externally exposed site on EGFR and does not simultaneously activate the receptor. In order to generate a high affinity EGFR-specific ligand that can be injected shortly before surgery, we searched for a low molecular weight protein scaffold that would exhibit high affinity and specificity for EGFR. In this paper we demonstrate that an EGFR-specific Centyrin, a novel class of protein scaffold molecules developed by O'Neil and coworkers,[17] provides the specificity of an antibody with the size (~10 kDa) and stability of a small organic molecule. Here we report the first application of a Centyrin for *in vivo* tumor imaging by conjugating the EGFR-specific Centyrin to a highly fluorescent near infrared (NIR) dye.

Results

Affinity determination of 83v2 binding to recombinant human and murine EGFR *in Vitro*

Binding affinities of 83v2 to murine or human EGFR were nearly identical with measured intrinsic affinity of 0.6 nM for either receptor. Thus, in a murine xenograft model, 83v2 is expected to bind both normal murine $EGFR^+$ tissues and human $EGFR^+$ tumor cells.

	kon (1/Ms)	koff(1/s)	KD (nM)
Human EGFR-Fc	5.30E+04	2.90E-05	0.55
Murine EGFR-Fc	4.99E+04	3.13E-05	0.63

Synthesis and characterization of Centyrin NIR dye conjugate (CNDC)

The low molecular weight Centyrin (83v2Cys) modified with a single cysteine for conjugation was selected as the targeting ligand for delivery of the near-infrared (NIR) dye (S0456) to EGFR positive tumors. As shown in Scheme 1, 83v2Cys was coupled to LMNIR2 in PBS buffer using maleimide chemistry. The final Centyrin-NIR dye conjugate was obtained in a total overall yield of 42%, purified by PD10 size exclusion column chromatography and named CNDC. The total molecular weight of the conjugate is 12814 Da and its fluorescence excitation and emission maxima are: λex = 770 nm, λem = 790 nm.

Analysis *of* CNDC Binding to HCC827 Cells *In Vitro*.

EGFR-positive HCC827 cells were used to evaluate EGFR-mediated binding and endocytosis of CNDC. As seen in Fig. 1, following incubation of HCC827 cells with 100 nM CNDC for 1 h at 37 °C, fluorescence is seen both on the surfaces and within the interiors of the cultured HCC827 cells. Moreover, upon co-incubation of the same cells with CNDC in the presence of excess Centyrin (83v2Cys), all cell surface and internal fluorescence is eliminated, suggesting that binding and uptake of the fluorescence seen in the absence of excess competing ligand is EGFR-mediated.

Quantitative analysis of EGFR-specific binding was conducted by measuring cell-associated fluorescence following incubation of the HCC827 cells with increasing concentrations of CNDC. As shown in Fig. 1B, binding was found to be saturable with an apparent dissociation constant of 1.4 nM (blue curve). Binding was also quantitatively inhibited when a 100-fold molar excess of unconjugated Centyrinwas co-incubated with the CNDC (red curve).

In Vivo Imaging and Biodistribution

In order to determine whether CNDC can specifically label EGFR-expressing tumors *in vivo*, mice with HCC827 xenografts were injected via the tail vein with 10 nmol CNDC and imaged over the subsequent 48 h period. As shown in Figure 2, tumor accumulation of CNDC began at 4 h and reached its peak fluorescence between 6 and 12 h.

To further assure that the fluorescent signal from the tumor was adequate for surgical applications, we next performed a model tumor resection surgery guided by the images obtained with CNDC. One such sequence of surgical procedures is shown Fig. 3. In this sequence, the tumor was initially located in the intact animal by NIR fluorescence whole body imaging (panel 1). Next, guided by this image, an incision made directly over the fluorescent locus to expose the tumor mass (panel 2). With continued aid of the NIR fluorescence image, the cancer tissue was carefully resected and placed to the right of the tumor-bearing mouse for further imaging (panel 3). Finally, to ensure that all malignant disease had been successfully removed, the sensitivity of the camera was increased and the animal was reimaged. As shown in panel 4, this subsequent image revealed the presence of a small pocket of residual cancer, which was then completed resected with the aid of the fluorescence image (tumor-free image not shown).

Live imaging indicated that stably retained fluorescence was primarily confined to the tumor and kidneys, and this was further confirmed when the major organs were excised at 48 h and imaged (Fig. 4). The elevated fluorescence in the kidneys and liver (Figure S4) may arise both from the known expression of EGFR in these two organs[58, 59] and the fact that both kidneys and liver constitute routes of CNDC excretion.

Based on the high affinity binding constant of 1.4 nM observed *in vitro*, we next explored whether lower doses of CNDC might also afford better images of solid tumors *in vivo*. For this purpose, tumor-bearing mice were injected via tail vein with either 5 or 1 nmol CNDC/mouse, and images were again collected as a function of time post-injection. As shown in Figs. S5 and S6, similar tumor selectivity was seen at 5 nmol/mouse, only the

background CNDC fluorescence cleared much faster at 1 nmol/mouse than at higher CNDC concentrations, allowing distinct visualization of the tumor by 1h post-injection. More importantly, analogous tumor-to-background ratios were also observed at 1 nmol/mouse, with good tumor resolution again obtained at the 1–2h time point (Fig. 5). Because uptake of fluorescence in the tumor was almost quantitatively blocked by co-administration of 100-fold excess unlabeled Centyrin, we conclude that tumor uptake of CNDC is EGFR-mediated. Moreover, since the majority of fluorescence accumulation in the kidneys could be similarly competed with excess unlabeled Centyrin, we also conclude that much of CNDC retention in the kidneys is EGFR-mediated. The fact that the majority of tumor-specific fluorescence is retained in the tumor mass for at least 24 h further argues that the lower 1 nmol/mouse dose is probably adequate for most applications in fluorescence-guided surgery.

To obtain an initial indication of the optimal time interval between CNDC injection and image acquisition, the pharmacokinetics of CNDC in live mice was examined. As shown in Fig. 6, analysis of the rise and fall of CNDC fluorescence in the blood following intravenous injection revealed that peak fluorescence was seen almost immediately and that clearance from the bloodstream proceeded with a half-life of ~4 hours resulting in nearly complete elimination by the ~48 h time point. Not surprisingly, lower initial doses of CNDC yielded better tumor:background ratios at longer time points for most organs (Fig. 7), again suggesting that the ideal dose of CNDC for fluorescence-guided surgery might lie at the lower end of those examined here.

Discussion

As discussed above, initial clinical trials aimed at examining the use of tumor-targeted fluorescent dyes for identification and resection of malignant lesions during cancer surgery have yielded promising results.[5–9] Buoyed by these data, an increase in research aimed at developing additional tumor-targeted fluorescent dyes has ensued, yielding a dramatic expansion of the tools for fluorescence guided surgery.[11, 18–46] Not surprisingly, most new fluorescence imaging agents have relied on either activation of a quenched fluorescent dye by a tumor-specific enzyme[23–38] or binding of a ligand-conjugated dye by a tumor-specific receptor.[39–46] While several of the latter class of dyes have been developed for imaging cancers that over-express a folate receptor[5–11], neurokinin 1 receptor,[39] cholecystokinin 2 receptor,[40] prostate-specific membrane antigen receptor,[41–43] CXCR4 receptor,[44] and carbonic anhydrase IX[45–46] etc.,[47–56] other very tumor-specific proteins have not been targetable with small organic ligands, largely because they are either topographically too featureless, conformationally too flexible, or chemically too unreactive to bind small molecules with high affinity. Thus, to establish high affinity associations with such unreactive surfaces, larger ligands that can establish multiple weak interactions over large surface areas are thought to be essential. And while antibodies constitute the most readily recognized examples of such ligands, their large size has led to undesirable pharmacokinetic properties that significantly limit their use in intra-operative imaging.

In an attempt to identify a ligand as adaptable as an antibody but of considerably smaller size, we looked for a low molecular weight protein scaffold of human origin (i.e. for low

immunogenicity) with a stable 3-dimensional structure, good water solubility, low toxicity, single site for dye derivatization, and freely mutatable surface that could be genetically engineered to bind almost any cell surface protein. The Centyrin family of protein scaffolds met all of these requirements and the pre-existing Centyrin that was developed to recognize EGFR (83v2Cys[57]) constituted an ideal test system to assess the feasibility of using a protein scaffold for fluorescence-guided surgery. In this paper we have demonstrated that the Centyrin-NIR dye conjugate directed to EGFR yields very a good tumor:background ratio in minimal time following its intravenous injection. Except for its retention in the kidneys and liver (due to expression of EGFR in these organs)[58,59] and its slow clearance through the liver, the conjugate shows little accumulation in any healthy organs. Thus, for EGFR-positive cancers that neither reside nor metastasize to the kidneys or liver (e.g. cancers of the breast, bladder, colon, etc.)[60], CNDC should constitute a viable candidate for use in fluorescence-guided surgery. The fact that CNDC binds to human and murine EGFR with similar affinity further suggests that the healthy tissue distribution observed in this study should be representative of the healthy tissue uptake in humans.

Although insufficient data still exist to draw any firm conclusions, it might still be useful to begin to compare the properties of the first three major classes of ligand-conjugated fluorescent dyes that have been studied *in vivo* to date, namely: i) low molecular weight organic ligands (e.g. folic acid, M_R~ 441), ii) protein scaffolds (e.g. an EGFR-binding Centyrin, M_R~12,814), and iii) antibodies (e.g. an anti-EGFR antibody, M_R~150,000). From the limited published reports available to date, it would appear that the affinities of all three ligands for their tumor targets are somewhat similar, i.e. K_D ~10^{-9}M.[61, 62] Moreover, all three ligand types display some kidney and liver retention, likely due to a combination of receptor expression in those tissue and excretion mechanisms. While the immunogenicity potential of Centyrins has not yet been tested in humans, good stability, solubility and homogeneity properties have been reported[57]. Neverthess, several features distinguish Centyrins and antibodies from small molecule ligands. First, the binding regions of antibodies and Centyrins can be almost infinitely mutated to enable binding to most tumor-specific antigens (i.e. including receptors for which low molecular weight ligands are currently unavailable), whereas totally unique low molecular weight ligands must be designed for each different tumor-specific receptor.[39–46] Second, while the half-time for clearance of the anti-EGFR antibody appears to be several days in humans;[13,14] i.e. similar to the half-time for clearance of an anti-EGFR-drug conjugate in man,[15] the half-time for clearance of the EGFR-targeted Centyrin was found to be ~4h in mice (and will be somewhat longer in humans) and the half-times for clearance of both folate-fluorescein and folate-NIR dye conjugates in man are ~30 min. Based on established clinical data, the folate conjugates can be injected immediately prior to cancer surgery, with good contrast emerging within 1–2 hours of injection[5–11] while the antibody-dye conjugates must be administered several days prior to surgery to obtain good tumor contrast.[11] Given the more than eightfold slower clearance of the Centyrin conjugate than folate conjugate in mice, it remains uncertain whether our CNDC might be injected on the same day as surgery in man. However, with its eventual complete clearance from EGFR-negative tissues and its quantitative retention in the tumor mass for >24 h, a Centyrin-targeted NIR dye should

provide excellent tumor contrast when injected at least 6–8 h before initiation of cancer surgery in man.

Experimental Procedures

Chemicals

2-(1H-7-Azabenzotriazol-1-yl)-1,1,3,3-tetramethyl uronium hexafluorophosphate methanaminium (HATU) was obtained from Genscript Inc. (Piscataway, New Jersey). 3-(4-hydroxyphenyl)propionic acid, diisopropylethylamine (DIPEA), piperidine, dimethylsulphoxide (DMSO), isopropanol, and all other reagents were purchased from Sigma Aldrich. For the synthesis of LMNIR2-maleimide, 3-(4-hydroxyphenyl)propionic acid and N-(2-aminoethyl)maleimide trifluoroacetate salt were purchased from Sigma Aldrich and S0456 was obtained from Few Chemicals. The Centyrin 83v2Cys was provided by Janssen R&D. Murine EGFR-Fc was purchased from R&D Systems and human EGFR-Fc was prepared by Janssen R&D.

Synthesis of LMNIR2 and LMNIR2-Maleimide

The synthesis of both LMNIR2 and its maleimide conjugate (LMNIR2-Maleimide) was performed as shown in Scheme 1. The chloro near-infrared dye (S0456) was reacted with 3-(4-hydroxyphenyl)propionic acid in the presence of 2 equivlents of KOH, in dimethylsulphoxide (DMSO) at 60°C for 60 min to give compound LMNIR2 (near IR dye). The crude product was purified by preparative reverse-phase high-performance liquid chromatography (yield of 68% and final purity of 96%) with a gradient mobile phase consisting of 20 mM ammonium acetate buffer and 5% to 80% acetonitrile over 30 min (xTerra C18; Waters; 10 μm; 19 × 250 mm). Elution of the near IR dye, LMNIR2, was monitored at 280 nm, and the identities of eluted compounds were analyzed by liquid chromatography−mass spectrometry (see Figure S2 Supporting Information).

For synthesis of the maleimide conjugate of LMNIR2, LMNIR2 (1 equiv) dissolved in anhydrous DMSO containing diisopropylethylamine (5 equiv) and HATU (1 equiv) was stirred for 25 min under argon atmosphere. A 3-fold molar excess of N-(2-aminoethyl)maleimide trifluoroacetate salt was then added and stirred overnight at room temperature, as outlined in Scheme 1. The product was precipitated by addition of isopropanol and collected by centrifugation prior to redissolution in DMSO. The crude product was purified by preparative reverse phase HPLC using a mobile phase of A = 20 mM ammonium acetate buffer, pH 7; B = acetonitrile; gradient 0–50% B in 30 min, 13 mL/min, λ = 280 nm. Pure fractions were analyzed by LC-MS and (see Figure S3 in Supporting Information), pooled and lyophilized to furnish LMNIR2-Maleimide.

Synthesis of Centyrin NIR dye conjugate (CNDC)

The EGFR-specific Centyrin, 83v2Cys, was obtained by screening a Centyrin library[17] for Centyrins that exhibited high affinity for EGFR and then the selected Centyrin (100–200uM) was treated with 10 mM TCEP (a reducing agent) and incubated for 30–45 min at room temperature[58]. Excess TCEP was removed by incubation with 3 vol of ammonium sulfate (~4 M) on ice for 20 min followed by centrifugation at 25000 rpm for 20 min at 10°C.

After discarding the supernatant the 83v2Cys Centyrin was dissolved in aqueous buffer and same procedure was repeated to remove all traces of TCEP. The reduced Centyrin was then resuspended in ~3 volumes of ammonium sulfate:PBS mixture (3:1) and again incubated on ice. After centrifugation as above, the supernatant was again discarded and the final pellet was resuspended in PBS. The concentration of protein was then measured using a UV-Vis spectrophotometer assuming an extinction coefficient of 83v2Cys is 19180 mol^{-1} cm^{-1}. For conjugation of the Centyrin to LMNIR2-maleimide, 1.1 equivalents of the dye was added to the reduced centyrin in PBS and stirred gently at room temperature for 60 min (Scheme 1). The crude reaction mixture containing CNDC was purified by size-exclusion chromatography in PBS on a PD10 column using gravity flow. The final concentration of the 83v2Cys-LMNIR2 conjugate in PBS was measured by UV-Vis spectrophotometer using an extinction coefficient of 83v2Cys of 19180 mol^{-1} cm^{-1}.

Affinity determination of 83v2 binding to human and murine EGFR-Fc.

Binding affinity of 83v2 to recombinant human and murine EGFR, both with a C terminal human Fc fusion was measured using a ProteOn XPR-36 instrument (BioRad). Goat anti-human Fc IgG (R&D system) was directly immobilized via amine coupling at 5 μg/mL in acetate buffer, pH 5.0 on all 6 ligand channels in horizontal orientation on a GLC Sensor Chip (Bio-Rad, catalog no. 176–5011) with a flow rate of 30 μL/min in PBS containing 0.005% Tween-20. The immobilization densities averaged about 1500 Response Units (RU) with less than 5% variation among different channels. Human EGFR-Fc and murine EGFR-Fc were captured on the anti-Fc IgG surface each at 2 different concentrations 10, 5 ug/ml in vertical ligand orientation, with final captured level ranging 600~800 Rus. Two ligand channels were used as no antigen surface controls. 83v2 starting at 1uM in 3-fold dilution series of 5 concentrations flew in as analyte to bind to captured EGFRs in the horizontal orientation. A buffer sample was also injected to monitor the dissociation of captured EGFR-Fc and baseline stability. The dissociation phase for all concentrations of the Centryin was monitored at a flow rate of 100 μL/min for 60 minutes. The binding surface was regenerated for the next interaction cycle using a 18 second pulse of 0.8% phosphoric acid to remove the EGFR-Fc and bound Centyrin. The raw data were processed by subtracting two sets of reference data from the response data: 1) the inter-spot signals to correct for the non-specific interactions between the Centyrin and the empty chip surface; 2) the buffer channel signals to correct for baseline drifting due to the dissociation of captured EGFR-Fc ligand surface over time. The processed data at all concentrations for the Centyrin were globally fit to a 1:1 simple Langmuir binding model to extract estimates of the kinetic (k_{on}, k_{off}) and affinity (K_D) constants.

Analysis of 83v2Cys-LMNIR2 Conjugate Binding to HCC827 Cells

The EGFR-positive HCC827 cell line utilized in these studies was purchased from ATCC (Manassas, VA). HCC827 cells were cultured in RPMI medium supplemented with 10% fetal bovine serum and 1% penicillin streptomycin at 37 °C in a humidified 95% air 5% CO2 atmosphere. For analysis of the intracellular distribution of CNDC, HCC827 cells were seeded into a confocal dish at a density of 1 × 105 cells per well and allowed to grow to confluence. Cells were then incubated for 1 h at 37 °C with 100 nM of 83v2Cys-LMNIR2 in the presence or absence of 100-fold excess 83v2Cys and rinsed three times with 1 mL

of cell culture medium to remove unbound 83v2Cys-LMNIR2. 0.5 mL of fresh medium was then added to each well and images were obtained using a Nikon 90i Fluorescence Microscope. The translocation of fluorescent CNDC from the plasma membrane into intracellular organelles was then followed as a function of time.

For analysis of CNDC binding affinity, HCC827 cells were seeded into 24 well plates (BD Purecoat Amine, BD Biosciences) and allowed to grow to confluence over 48–72 h. Spent medium in each well was replaced with 0.5 mL of fresh medium containing 0.5% bovine serum albumin and increasing concentrations of the CNDC conjugate in the presence or absence of 100-fold excess of 83v2Cys were added. After incubation for 1h at 37 °C, cells were rinsed with incubation solution (2 × 1.0 mL) to remove unbound fluorescence and the washed cells were dissolved in 0.5 mL of 1% aqueous sodium dodecyl sulfate. Cell associated fluorescence was then determined by measuring emission of the resulting solution upon excitation at 755 nm. All experiments were performed in triplicate. The dissociation constant (K_D) was calculated from a plot of cell bound fluorescence (a.u.) versus the concentration of fluorescent conjugate added using Graphpad Prism software and assuming a noncooperative single site binding equilibrium.

Generation of Subcutaneous Tumor Using HCC827 Cells in Mice

Athymic female nu/nu mice were purchased from Harlan Laboratories (Indianapolis, IN), maintained on normal rodent chow and housed in a sterile environment on a standard 12 h light and dark cycle for the duration of the study. All animal procedures were approved by the Purdue Animal Care and Use Committee in accordance with NIH guidelines.

Six week old mice were inoculated subcutaneously on their shoulders using a 25-gauge needle with HCC827 cells (5.0×10^6 cells/mouse) suspended in 200 μL of culture medium. Growth of the tumors was measured in two perpendicular directions every 2 days using a caliper, and the volumes of the tumors were calculated as $0.5 \times L \times W^2$ (L = measurement of longest axis, and W = measurement of axis perpendicular to L in millimeters). Animals were imaged when the tumors reached 300–400 mm^3 volume (~4 weeks). Experiments on live mice involved at least three mice per group.

Fluorescence Imaging and Analysis of Mice

Tumor-bearing mice were treated via tail vein injection with various concentrations of dye conjugate in the presence or absence of a 100-fold excess of 83v2Cys to block all unoccupied EGFR binding sites. Mice were imaged up to 48 h post injection using a Caliper IVIS Lumina II Imaging station coupled to a ISOON5160 Andor Nikon camera equipped with Living Image Software Version 4.0. The settings were as follows: lamp level, high; excitation, 745 nm; emission, ICG; epi illumination; binning (M) 4; FOV, 12.5; f-stop, 4; acquisition time, 1 s.

Pharmacokinetics of CNDC in nude mice

After IV administration of 10 nmol of CNDC, the CNDC concentration in the blood was measured over the subsequent 48 h using a Caliper IVIS Lumina II Imaging station coupled to a ISOON5160 Andor Nikon camera equipped with Living Image Software Version 4.0.

Supplementary Material

Refer to Web version on PubMed Central for supplementary material.

Acknowledgements

This work was supported in part by a grant from NIH R01 CA193556 (Singhal, Low), On Target Laboratories and Janssen R&D.

References

1. Nguyen QT, Tsien RY (2013) Fluorescence-guided surgery with live molecular navigation--a new cutting edge. Nat. Rev. Cancer 13, 653–662. [PubMed: 23924645]
2. Wu M, Gunning W, Ratnam M. (1999) Expression of folate receptor type alpha in relation to cell type, malignancy, and differentiation in ovary, uterus, and cervix. Cancer Epidemiol Biomarkers Prev. 8, 775–782. [PubMed: 10498396]
3. Parker N, Turk MJ, Westrick E, Lewis JD, Low PS, Leamon CP (2005) Folate receptor expression in carcinomas and normal tissues determined by a quantitative radioligand binding assay. Anal. Biochem. 338, 284–293. [PubMed: 15745749]
4. Kalli KR, Oberg AL, Keeney GL, Christianson TJ, Low PS, Knutson KL, Hartmann LC (2008) Folate receptor alpha as a tumor target in epithelial ovarian cancer. Gynecol Oncol. 108, 619–626. [PubMed: 18222534]
5. van Dam GM, Themelis G, Crane LM, Harlaar NJ, Pleijhuis RG, Kelder W, Sarantopoulos A, de Jong JS, Arts HJ, van der Zee AG, et al. (2011) Intraoperative tumor-specific fluorescence imaging in ovarian cancer by folate receptor-alpha targeting: first in-human results. Nat. Med. 17, 1315–1319. [PubMed: 21926976]
6. Hoogstins CES, Tummers QRJG, Gaarenstroom KN, de Kroon CD, Trimbos BMJ, Bosse T, Vincent THBM, Smit Jaap Vuyk, van de Velde CJH, Cohen AF, et al. (2016) Novel Tumor-Specific Agent for Intraoperative Near-Infrared Fluorescence Imaging: A translational study in healthy volunteers and patients with ovarian cancer. Clin Cancer Res 22, 2929–2938. [PubMed: 27306792]
7. Kçnig SG, Roland Kramer R. (2017) Accessing structurally diverse near-infrared cyanine dyes for folate receptor-targeted cancer cell staining. Chem. Eur. J. 23, 9306–9312 [PubMed: 28339120]
8. Jesus ED, Keating JJ, Kularatne SA, Jiang J, Judy R, Predina J, Nie S, Low PS, Singhal S. (2015) Comparison of folate receptor targeted optical contrast agents for intraoperative molecular imaging. International Journal of Molecular Imaging Article ID 469047, 10 pages.
9. Shum CF, Bahler CD, Low PS, Ratliff TL, Kheyfets SV, Natarajan JP, Sandusky GE, Sundaram CP (2016) Novel use of folate-targeted intraoperative fluorescence, OTL38, in Robot-Assisted Laparoscopic Partial Nephrectomy: Report of the First Three Cases. J Endourol Case Rep 2, 189–197. [PubMed: 27868096]
10. Keating JJ, Okusanya OT, De Jesus E, Judy R, Jiang J, Deshpande C, Nie S, Low PS, Singhal S. (2016) Intraoperative molecular imaging of lung adenocarcinoma can identify residual tumor cells at the surgical margins. Mol Imaging Biol 18, 209–218. [PubMed: 26228697]
11. Kennedy GT, Okusanya OT, Keating JJ, Heitjan DF, Deshpande C, Litzky L, Albelda SM, Drebin JA, Nie S, Low PS, Singhal S. (2015) The optical biopsy: A novel technique for rapid intraoperative diagnosis of primary pulmonary adenocarcinomas. Ann Surg 262, 602–609. [PubMed: 26366539]
12. Sebastian S, Settleman J, Reshkin SJ, Azzariti A, Bellizzi A, Paradiso A. (2006) The complexity of targeting EGFR signalling in cancer: from expression to turnover. Biochim Biophys Acta 1766, 120–139. [PubMed: 16889899]
13. Nicholson RI, Gee JM, Harper ME (2001) EGFR and cancer prognosis. Eur J Cancer 37: Suppl 4, S9–15. [PubMed: 11597399]
14. Miao Z, Ren G, Liu H, Jiang L, Cheng Z. (2010) Cy5.5-labeled affibody molecule for near-infrared fluorescent optical imaging of epidermal growth factor receptor positive tumors. J. Biomed. Opt. 5, 036007.

15. Warram JM, de Boer E, Sorace AG, Chung TK, Kim H, Pleijhuis RG, van Dam GM, Rosenthal EL (2014) Antibody-based imaging strategies for cancer. Cancer Metastasis Rev 33, 809–822. [PubMed: 24913898]

16. Peters C, Brown S. (2015) Antibody–drug conjugates as novel anti-cancer chemotherapeutics. Biosci Rep 35, e00225.

17. Diem MD, Hyun L, Yi F, Hippensteel R, Kuhar E, Lowenstein C, Swift EJ, O'Neil KT, Jacobs SA (2014) Selection of high-affinity Centyrin FN3 domains from a simple library diversified at a combination of strand and loop positions. Protein Eng Des Sel 27, 419–429. [PubMed: 24786107]

18. Garland M, Yim JJ, Bogyo MA (2016) Bright future for precision medicine: Advances in fluorescent chemical probe design and their clinical application. Cell Chemical Biology 23, 122–136. [PubMed: 26933740]

19. Zhang RR, Schroeder AB, Grudzinski JJ, Rosenthal EL, Warram JM, Pinchuk AN, Eliceiri KW, Kuo JS, Weichert JP (2017) Beyond the margins: real-time detection of cancer using targeted fluorophores. Nat. Rev. Clin. Oncol 1–18.

20. Hong G, Antaris AL, Dai H. (2017) Near-infrared fluorophores for biomedical imaging. Nat. Biomed. Eng. 1, 0010.

21. Vahrmeijer AL, Hutteman M, van der Vorst JR, van de Velde CJH, Frangioni JV (2013) Image-guided cancer surgery using near-infrared fluorescence. Nat. Rev. Clin. Oncol 10, 507–518. [PubMed: 23881033]

22. Okusanya OT, Brian Madajewski BA, Segal E, Judy BF, Venegas OG, Judy R,P., Quatromoni JG, Wang MD, Nie S, Singhal S. (2015) Small portable interchangeable imager of fluorescence for fluorescence guided surgery and research. Technol Cancer Res Treat 14, 213–220. [PubMed: 24354756]

23. Bromme DWS (2011) Role of cysteine cathepsins in extracellular proteolysis. In Extracellular Matrix Degradation, Mecham W.C.P.a.R.P., ed. (Springer Berlin Heidelberg), pp. 23–51.

24. Mohamed MM, Sloane BF (2006) Cysteine cathepsins: multifunctional enzymes in cancer. Nat. Rev. Cancer 6, 764–775. [PubMed: 16990854]

25. Powers JC, Asgian JL, Ekici OD, James KE (2002) Irreversible inhibitors of serine, cysteine, and threonine proteases. Chem. Rev. 102, 4639–4650. [PubMed: 12475205]

26. Blum G, Mullins SR, Keren K, Fonovic M, Jedeszko C, Rice MJ, Sloane BF, Bogyo M. (2005) Dynamic imaging of protease activity with fluorescently quenched activity-based probes. Nat. Chem. Biol 1, 203–209. [PubMed: 16408036]

27. Blum G, von Degenfeld G, Merchant MJ, Blau HM, Bogyo M. (2007) Noninvasive optical imaging of cysteine protease activity using fluorescently quenched activity-based probes. Nat. Chem. Biol 3, 668–677. [PubMed: 17828252]

28. Verdoes M, Oresic Bender K, Segal E, van der Linden WA, Syed S, Withana NP, Sanman LE, Bogyo M. (2013) Improved quenched fluorescent probe for imaging of cysteine cathepsin activity. J. Am. Chem. Soc 135, 14726–14730. [PubMed: 23971698]

29. Edgington LE, Berger AB, Blum G, Albrow VE, Paulick MG, Lineberry N, Bogyo M. (2009) Noninvasive optical imaging of apoptosis by caspase-targeted activity-based probes. Nat. Med 15, 967–973. [PubMed: 19597506]

30. Segal E, Prestwood TR, van der Linden WA, Carmi Y, Bhattacharya N, Withana N, Verdoes M, Habtezion A, Engleman EG, Bogyo M. (2015) Detection of intestinal cancer by local, topical application of a quenched fluorescence probe for cysteine cathepsins. Chem. Biol 22, 148–158. [PubMed: 25579207]

31. Bender OK, Ofori L, van der Linden WA, Mock ED, Datta GK, Chowdhury S, Li H, Segal E, Sanchez Lopez M, Ellman JA (2015) Design of a highly selective quenched activity-based probe and its application in dual color imaging studies of cathepsin S activity localization. J. Am. Chem. Soc 137, 4771–4777. [PubMed: 25785540]

32. Verdoes M, Edgington LE, Scheeren FA, Leyva M, Blum G, Weiskopf K, Bachmann MH, Ellman JA, Bogyo M. (2012) A nonpeptidic cathepsin S activity-based probe for noninvasive optical imaging of tumorassociated macrophages. Chem. Biol 19, 619–628. [PubMed: 22633413]

33. Cutter JL, Cohen NT, Wang J, Sloan AE, Cohen AR, Panneerselvam A, Schluchter M, Blum G, Bogyo M, Basilion JP (2012) Topical application of activity-based probes for visualization of brain tumor tissue. PLoS One 7, e33060.
34. Weissleder R, Tung CH, Mahmood U, and Bogdanov A Jr. (1999) In vivo imaging of tumors with protease-activated near-infrared fluorescent probes. Nat. Biotechnol 17, 375–378. [PubMed: 10207887]
35. Hu HY, Vats D, Vizovisek M, Kramer L, Germanier C, Wendt KU, Rudin M, Turk B, Plettenburg O, Schultz C. (2014) In vivo imaging of mouse tumors by a lipidated cathepsin S substrate. Angew. Chem. Int. Ed. Engl 53, 7669–7673. [PubMed: 24888522]
36. Ofori LO, Withana NP, Prestwood TR, Verdoes M, Brady JJ, Winslow MM, Sorger J, Bogyo M. (2015) Design of protease activated optical contrast agents that exploit a latent lysosomotropic effect for use in fluorescence-guided surgery. ACS Chem. Biol 10, 1977–1988. [PubMed: 26039341]
37. Savariar EN, Felsen CN, Nashi N, Jiang T, Ellies LG, Steinbach P, Tsien RY, Nguyen QT (2013) Real-time in vivo molecular detection of primary tumors and metastases with ratiometric activatable cell-penetrating peptides. Cancer Res 73, 855–864. [PubMed: 23188503]
38. Ye D, Shuhendler AJ, Cui L, Tong L, Tee SS, Tikhomirov G, Felsher DW, Rao J. (2014) Bioorthogonal cyclization-mediated in situ self-assembly of small-molecule probes for imaging caspase activity *in vivo*. Nat. Chem 6, 519–526. [PubMed: 24848238]
39. Kanduluru A, Srinivasarao M, Low PS (2016) Design, synthesis, and evaluation of a neurokinin-1 receptor targeted near-IR dye for fluorescence-guided surgery of neuroendocrine cancers. Bioconjugate Chem 27, 2157–2165.
40. Wayua C, Low PS (2014) Evaluation of a cholecystokinin 2 receptor-targeted near-infrared dye for fluorescence-guided surgery of cancer. Mol. Pharmaceutics 11, 468–476.
41. Banerjee SR, Pullambhatla M, Byun Y, Nimmagadda S, Foss CA, Green G, Fox JJ, Lupold SE, Mease RC, Pomper MG (2011) Sequential SPECT and optical imaging of experimental models of prostate cancer with a dual modality inhibitor of the prostate-specific membrane antigen. Angew. Chem. Int. Ed. Engl 50, 9167–9170. [PubMed: 21861274]
42. Chen Y, Dhara S, Banerjee SR, Byun Y, Pullambhatla M, Mease RC, Pomper MG (2009) A low molecular weight PSMA-based fluorescent imaging agent for cancer. Biochem. Biophys. Res. Commun 390, 624–629. [PubMed: 19818734]
43. Neuman BP, Eifler JB, Castanares M, Chowdhury WH, Chen Y, Mease RC, Ma R, Mukherjee A, Lupold SE, Pomper MG (2015) Real-time, near-infrared fluorescence imaging with an optimized dye/ light source/camera combination for surgical guidance of prostate cancer. Clin. Cancer Res 21, 771–780. [PubMed: 25501577]
44. Guan G, Lu Y, Zhu X, Liu L, Chen J, Ma Q, Zhang Y, Wen Y, Yang L, Liu T, et al. (2015) CXCR4-targeted near-infrared imaging allows detection of orthotopic and metastatic human osteosarcoma in a mouse model. Sci. Rep 5, 15244. [PubMed: 26472699]
45. Lv PC, Roy J, Putt KS, Low PS (2016) Evaluation of a carbonic anhydrase IX-targeted near-infrared dye for fluorescence-guided surgery of hypoxic tumors. Mol Pharm 13, 1618–1625. [PubMed: 27043317]
46. Groves K, Bao B, Zhang J, Handy E, Kennedy P, Cuneo G, Supuran CT, Yared W, Peterson JD, Rajopadhye M. (2012) Synthesis and evaluation of near-infrared fluorescent sulfonamide derivatives for imaging of hypoxia-induced carbonic anhydrase IX expression in tumors. Bioorg. Med. Chem. Lett 22, 653–657. [PubMed: 22079760]
47. Chen X, Conti PS, Moats RA (2004) In vivo near-infrared fluorescence imaging of integrin αvβ3 in brain tumor xenografts. Cancer Res 64, 8009–8014. [PubMed: 15520209]
48. Choi HS, Gibbs SL, Lee JH, Kim SH, Ashitate Y, Liu F, Hyun H, Park G, Xie Y, Bae S, Henary M, Frangioni JV (2013) Targeted zwitterionic near-infrared fluorophores for improved optical imaging. Nat Biotechnol 31, 148–153. [PubMed: 23292608]
49. Verbeek FP, van der Vorst JR, Tummers QR, Boonstra MC, de Rooij KE, Löwik CW, Valentijn AR, van de Velde CJ, Choi HS, Frangioni JV, et al. (2014) Near-infrared fluorescence imaging of both colorectal cancer and ureters using a low-dose integrin targeted probe. Ann Surg Oncol 21, Suppl 4:S528–537. [PubMed: 24515567]

50. Boonstra MC, van Driel PB, van Willigen DM, Stammes MA, Prevoo HA, Tummers QR, Mazar AP, Beekman FJ, Kuppen PJ, van de Velde CJ et al. (2015) uPAR-targeted multimodal tracer for pre- and intraoperative imaging in cancer surgery. Oncotarget 6, 14260–14273. [PubMed: 25895028]
51. Christensen A, Juhl K, Persson M, Charabi BW, Mortensen J, Kiss K, Lelkaitis G, Rubek N, von Buchwald C, Kjær A. (2017) uPAR-targeted optical near-infrared (NIR) fluorescence imaging and PET for image-guided surgery in head and neck cancer: proof-of-concept in orthotopic xenograft model. Oncotarget, 8,15407–15419. [PubMed: 28039488]
52. Boonstra MC, Tolner B, Schaafsma BE, Boogerd LS, Prevoo HA, Bhavsar G, Kuppen PJ, Sier CF, Bonsing BA, Frangioni JV, et al. (2015) Preclinical evaluation of a novel CEA-targeting near-infrared fluorescent tracer delineating colorectal and pancreatic tumors. Int. J. Cancer 137, 1910–1920. [PubMed: 25895046]
53. van Driel PB, Boonstra MC, Prevoo HA, van de Giessen M, Snoeks TJ, Tummers QR, Keereweer S, Cordfunke RA, Fish A, van Eendenburg JD, et al. (2016) EpCAM as multi-tumour target for near-infrared fluorescence guided surgery. BMC Cancer 16, 884. [PubMed: 27842504]
54. He J, Yang L, Yi W, Fan W, Yu Wen., Miao X, Xiong L. (2017) Combination of fluorescence-guided surgery with photodynamic therapy for the treatment of cancer. Mol Imaging. 16, 1–15.
55. Jo D, Hyun H. (2017) Structure-inherent targeting of near-infrared fluorophores for image-guided surgery. Chonnam Med J. 53, 95–102. [PubMed: 28584787]
56. Liu J, Chen C, Ji S, Liu Q, Ding D, Zhaoa D, Liu B. (2017) Long wavelength excitable near-infrared fluorescent nanoparticles with aggregation-induced emission characteristics for image-guided tumor resection. Chem Sci. 8, 2782–2789. [PubMed: 28553514]
57. Goldberg SD, Cardoso RMF, Lin T, Spinka-Doms T, Klein D, Jacobs SA, Dudkin V, Gilliland G, O'Neil KT (2016) Engineering a targeted delivery platform using Centyrins. Protein Engineering, Design & Selection 563–572.
58. Melenhorst WB, Mulder GM, Qi Xi, Hoenderop JGJ, Kimura K, Eguchi S, Goor HV (2008) Epidermal Growth Factor Receptor Signaling in the Kidney. Hypertension 52, 987–993. [PubMed: 18981331]
59. Anuradha N, Wagner B, Sibilia M. (2007) The EGF receptor is required for efficient liver regeneration. Proc Natl Acad Sci USA 104, 17081–17086. [PubMed: 17940036]
60. Metastatic Cancer - National Cancer Institute [online], https://www.cancer.gov/types/metastatic-cancer. February 6, 2017.
61. Imai K,Takaoka A. (2006) Comparing antibody and small-molecule therapies for cancer. Nat Rev Cancer 6, 714–727. [PubMed: 16929325]
62. Vazquez-Lombardi R, Phan TG, Zimmermann C, Lowe D, Jermutus L, Christ D. (2015) Challenges and opportunities for non-antibody scaffold drugs. Drug Discov Today 20, 1271–1283. [PubMed: 26360055]

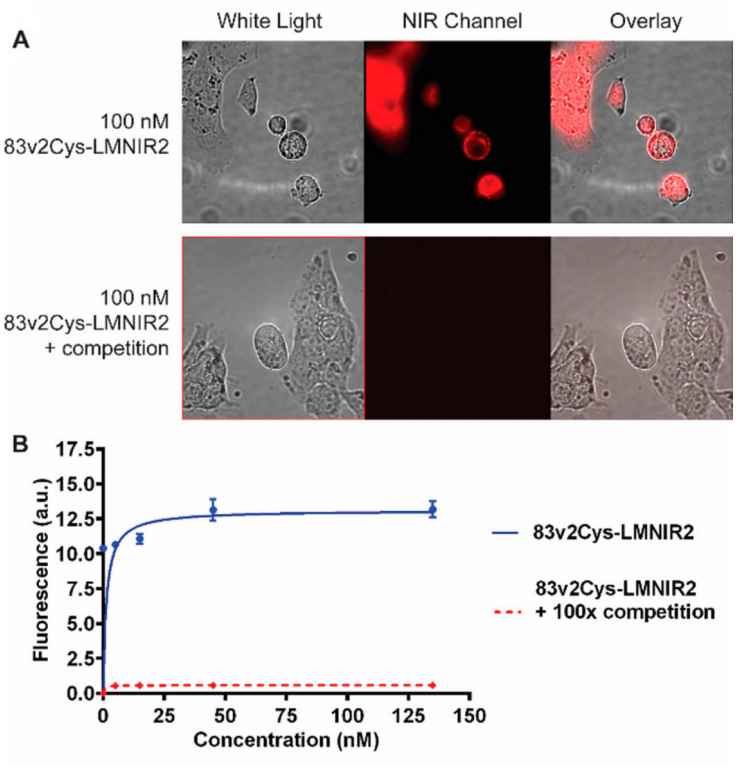

Figure 1.

Binding of the Centyrin near-infrared dye conjugate (CNDC) to HCC827 cells. **(A)** HCC827 cells were incubated with 100 nM CNDC in the presence or absence to 100-fold excess of CNDC (83v2Cys). **(B)** HCC827 cells were incubated with increasing concentrations of CNDC in the presence or absence to 100-fold excess of unlabeled Centyrin, 83v2Cys. Data are mean ± SEM of n=3.

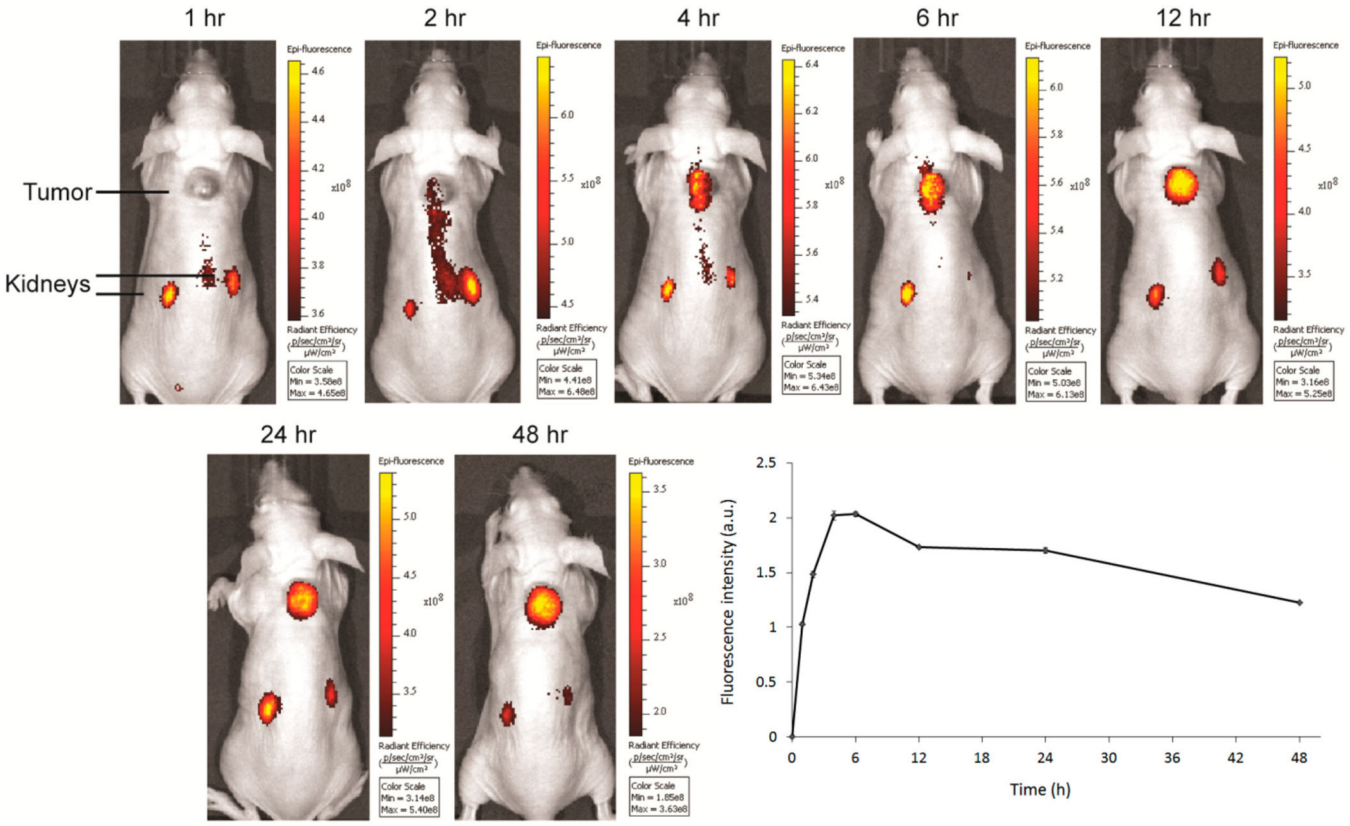

Figure 2.

Representative images of HCC827 tumor bearing mice treated with 10 nmol CNDC. Mice were injected via tail vein with 10 nmol CNDC and fluorescence images were acquired over a 48 h period. The graph shows mean fluorescence intensity ± SD for tumors from 3 mice.

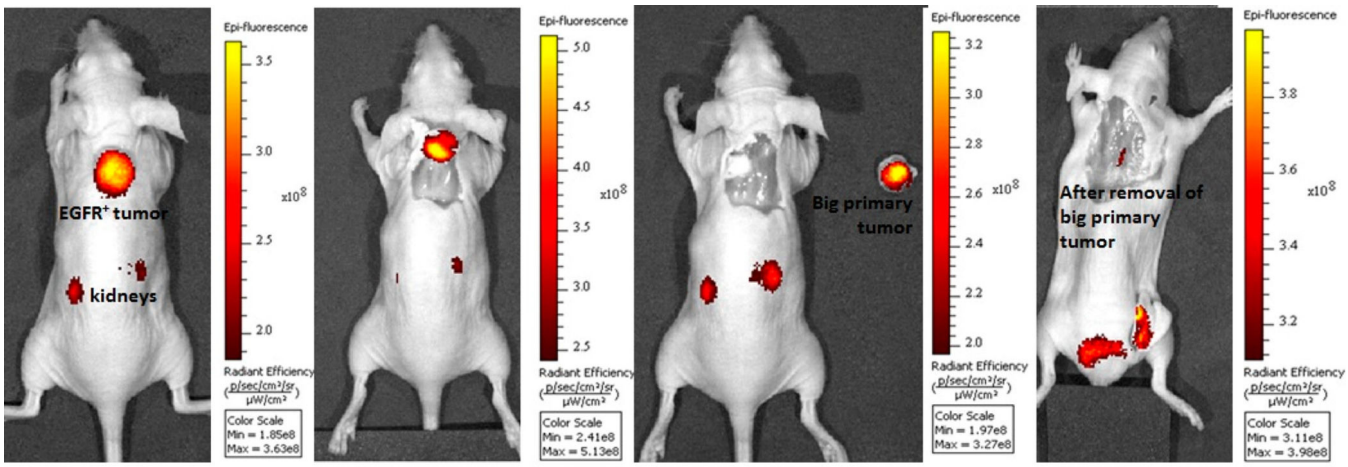

Figure 3.

Fluorescence guided surgery of HCC827 tumor bearing mice treated with 10 nmol CNDC injected via tail vein. Fluorescence images were acquired after 48 h and resected the cancer tissue by fluorescence guided sequence of surgical procedures. Ideal location for making an incision (panel 1); performed the incision and exposed the fluorescent mass (panel 2); resected the cancer tissue and placed the resected mass to the right of the tumor-bearing mouse (panel 3) and subsequent image revealed the presence of a small pocket of residual cancer (panel 4).

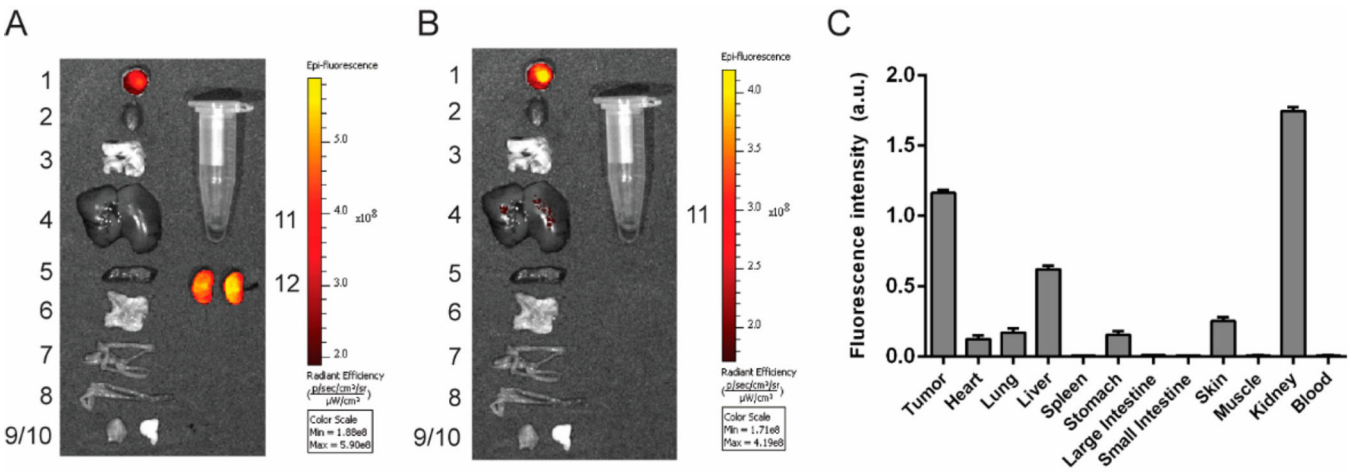

Figure 4.

Evaluation of CNDC (10 nmol) accumulation in the internal tissues and organs of the HCC827 tumor bearing mice. Organs and tissues were dissected at 48 h, and panels show **(A)** all organs and **(B)** organs excluding kidneys. Organs are labeled as follows: 1) tumor, 2) heart, 3) lungs, 4) liver, 5) spleen, 6) stomach, 7) small intestine, 8) large intestine, 9) muscle, 10) skin, 11) blood, 12) kidneys. **(C)** Quantification of tissue fluorescence intensity. Data are mean ± SD for 3 mice.

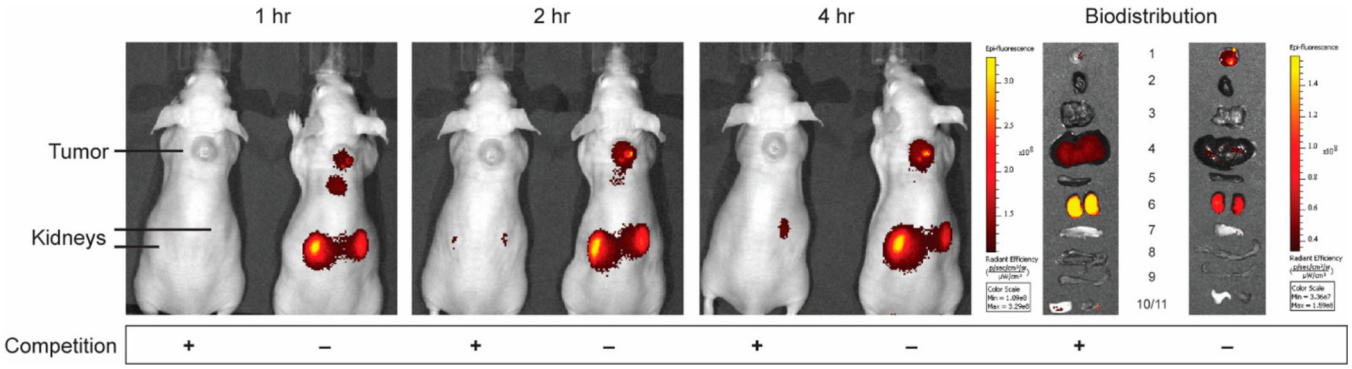

Figure 5.

Representative images of HCC827 tumor-bearing mice treated with 1 nmol CNDC in the presence or absence of competing unlabeled Centyrin. Mice were injected via tail vein with 1 nmol CNDC in the presence or absence of a 100-fold excess of 83v2Cys to block all vacant receptor binding sites and fluorescence images were acquired over the ensuing 4 h. Organs and tissues were resected after whole animal imaging at 4 h and are labeled as follows: 1) tumor, 2) heart, 3) lungs, 4) liver, 5) spleen, 6) kidneys, 7) stomach, 8) small intestine, 9) large intestine, 10) skin, 11) muscle.

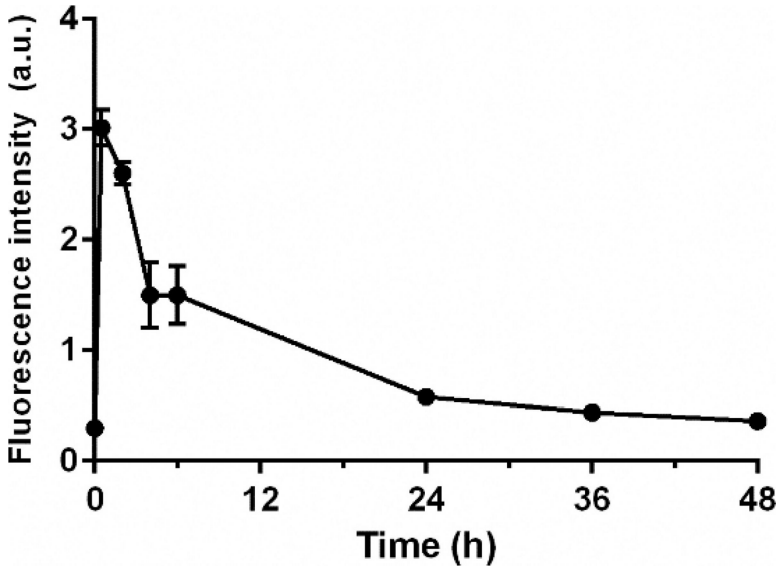

Figure 6.

Blood half-life of CNDC in vivo. 10 nmol CNDC were administered intravenously and blood samples were collected over 48 h. The graph shows mean fluorescence intensity ± SD for 3 mice.

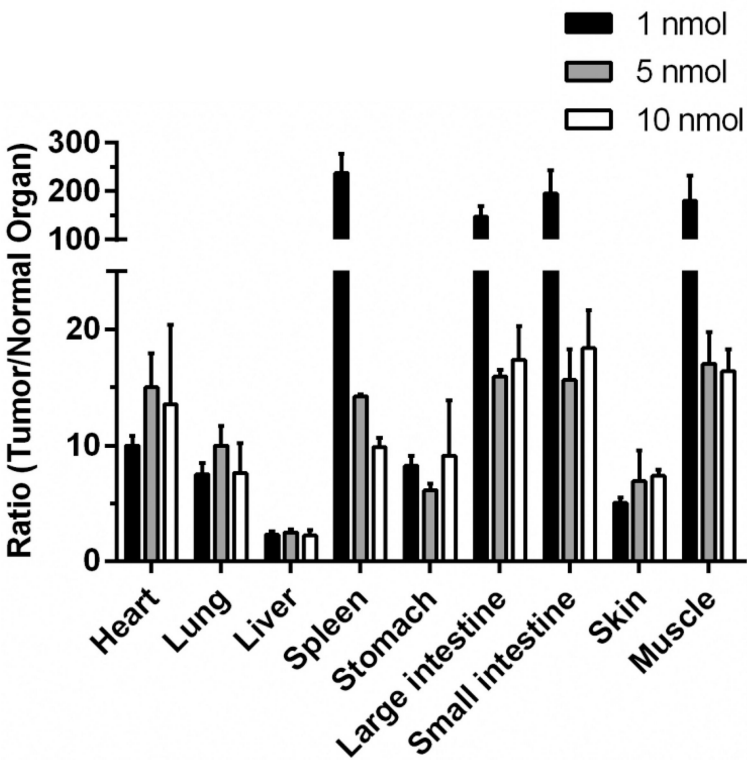

Figure 7.

Ratio of fluorescence intensity in tumor/normal organs in HCC827 tumor bearing mice dosed with 1 (100μL of 10μM), 5 (100μL of 50μM), or 10 (100μL of 100μM) nmol of CNDC. Mice were injected via tail vein with the indicated concentrations of CNDC and fluorescence images were acquired 4 h (1 nmol), 24 h (5 nmol) and 48 h (10 nmol) postinjection. Data are mean ± SD of n=3.

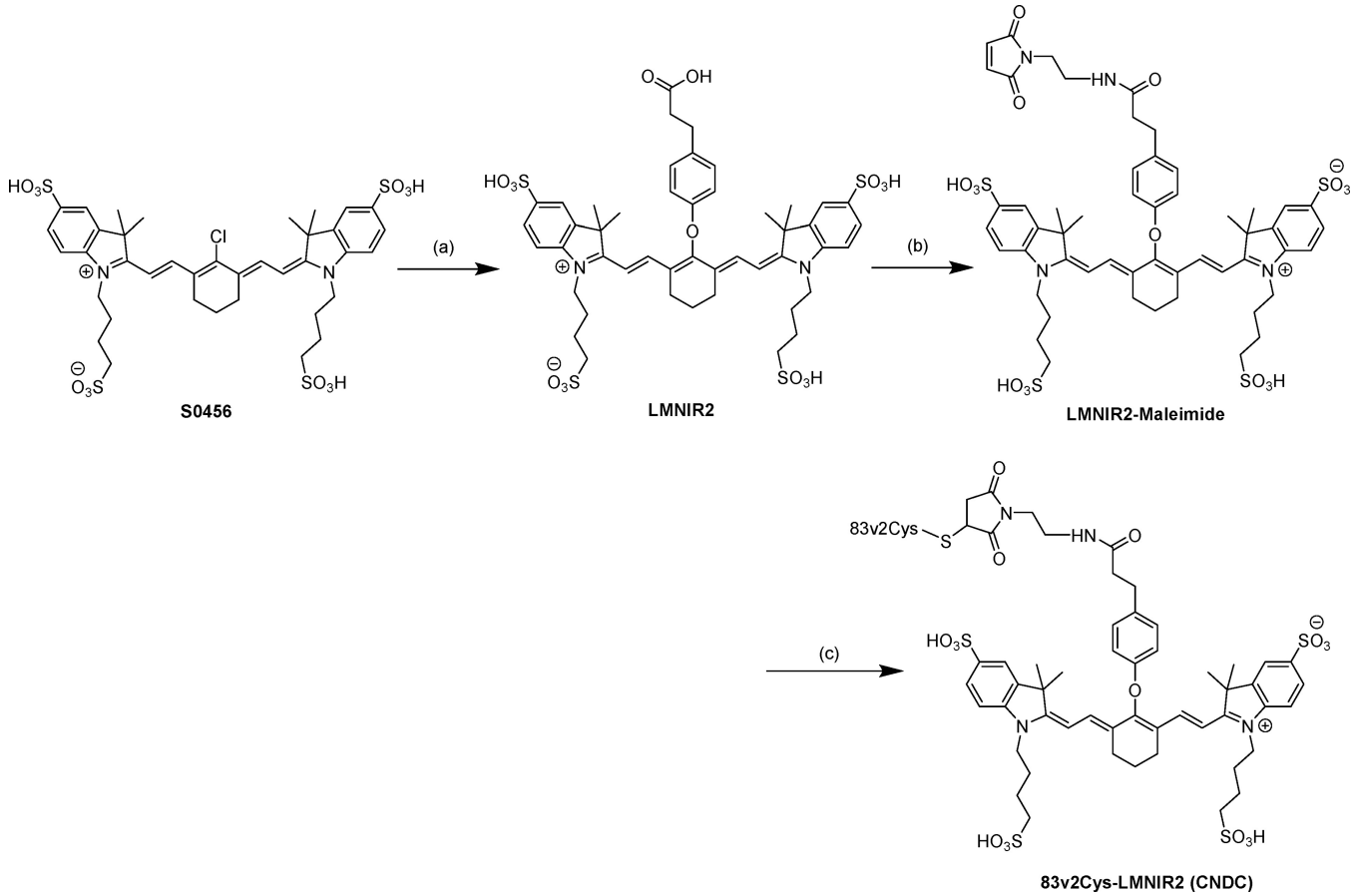

Scheme 1.

Synthesis of the Centyrin near-infrared dye labeling reagent[a]

[a]Reagents and conditions: (a) 3-(4-Hydroxyphenyl)propionic acid, KOH (2 equiv), DMSO, 60°C, 60 min (b) (i) HATU, DIPEA, DMSO, r.t. 25 min, (ii) N-(2-aminoethyl)malemide trifluoroacetate salt (2 equiv) stir overnight, (iii) isopropanol, centrifugation; (c) PBS and gentle mixing for 60 min